AGU PUBLICATIONS

Geophysical Research Letters

RESEARCH LETTER
10.1002/2015GL066728

Key Points:
- First comprehensive measurements of ice thickness in Patagonia with 1 to 1.5 km thick ice
- Gravity surveys are a critical complement to radar sounding surveys in Patagonia
- The results provide information about past, recent, and future glacier changes in Patagonia

Supporting Information:
- Supporting Information S1

Correspondence to:
E. Rignot,
erignot@uci.edu

Citation:
Gourletm, P., E. Rignot, A. Rivera, and G. Casassa (2016), Ice thickness of the northern half of the Patagonia Icefields of South America from high-resolution airborne gravity surveys, *Geophys. Res. Lett.*, *43*, 241–249, doi:10.1002/2015GL066728.

Received 23 OCT 2015
Accepted 30 NOV 2015
Accepted article online 4 DEC 2015
Published online 14 JAN 2016

Ice thickness of the northern half of the Patagonia Icefields of South America from high-resolution airborne gravity surveys

P. Gourlet[1], E. Rignot[1,2], A. Rivera[3], and G. Casassa[4,5]

[1]Department Earth System Science, University of California, Irvine, California, USA, [2]Jet Propulsion Laboratory, California Institute of Technology, Pasadena, California, USA, [3]Centro Estudios de Cientificos, Valdivia, Chile, [4]Geoestudios, San José de Maipo, Chile, [5]GAIA-Antártica, Universidad de Magallanes, Punta Arenas, Chile

Abstract We employ high-resolution, high-precision, helicopter-borne gravity observations of the Northern (NPI) and Southern Patagonia Icefields (SPI), South America, to infer ice thickness and bed topography using a three-dimensional model constrained by Fjord and lake bathymetry, and a land-ice mask. The results reveal thicker ice than the reflecting horizon of radar sounders, with 1 km deep ice for Glaciar San Rafael and Colonia (NPI) and 1.5 km deep ice for Glaciar Occidental (SPI). These bedrock troughs channelize fast motion of ice from the plateaus. Combining ice motion and thickness, we calculate balance accumulation levels of 3–6 m/yr water equivalent for the plateaus. Bed elevation remains below sea/lake level 15–20 km inland for Jorge Montt and O'Higgins, which favors retreat, and is at sea level for San Rafael, which halted its retreat. The results demonstrate the utility of airborne gravity surveys for providing critical data on ice volume, bed elevation, and balance accumulation of temperate ice masses.

1. Introduction

The Patagonia Icefields of South America are the largest icefields in the Southern Hemisphere outside of Antarctica [e.g., *Rivera et al.*, 2007; *Glasser et al.*, 2011]. The icefields have been losing mass over the last century, and the mass loss has been increasing with time [e.g., *Rignot et al.*, 2003; *Willis et al.*, 2012a, 2012b]. We distinguish the Northern Patagonia Icefield (NPI) with an area of 4000 km^2 at a center latitude of 47°S and 30 major outlet glaciers, and the Northern Patagonia Icefield (SPI) with an area of 11,056 km^2 at a center latitude of 49°S and 46 major glaciers [e.g., *Mouginot and Rignot*, 2014]. Glaciar San Rafael is the lowest latitude tidewater glacier in the world and the only marine-terminating glacier in NPI. Other NPI glaciers calve in proglacial lakes or are land terminating [*Rivera et al.*, 2007]. In the SPI, Glaciar Jorge Montt is among several glaciers (e.g., Témpano, Pío XI, HPS10 to HPS19, Penguin, Europa, HPS29, HPS31, Calvo, Asia, Amalia) that terminate in the ocean on the west coast, while others terminate in proglacial lakes [*Casassa et al.*, 2014; *Sakakibara and Sugiyama*, 2014]. Glaciers ending on the eastern side of SPI terminate in freshwater lakes (e.g., Lucía, Bravo, O'Higgins, Viedma, Upsala, Moreno, Grey, and Tyndall) or on land.

The total volume of the icefields is not known at present. A gravity traverse conducted in the 1980s indicated up to 1.5 km of ice on NPI [*Casassa*, 1987]. Radar sounders have had little success in measuring ice thickness in Patagonia, particularly in the interior of the plateau due to high absorption and scattering of temperate ice. Ground radars operating at MHz center frequencies have been limited to thicknesses of about 700–750 m of ice [*Rivera and Casassa*, 2002; *Raymond et al.*, 2005]. No measurement of ice thickness exists on the main SPI plateau where the deepest ice resides. Only a few glacier depth profiles have been collected with ground radar in the eastern-central part of the SPI at Glaciar Chico, with a maximum depth of 650 m [*Rivera and Casassa*, 2002]. Seismic methods have been used to measure the cross section of Glaciar Moreno, Argentina, with a maximum depth of 720 m [*Rott et al.*, 1998].

Gravimeters used to infer ice thickness in the early days of ice sheet exploration have been rapidly replaced by airborne radar sounding techniques which provide higher vertical precision, denser spatial sampling, and wider spatial coverage [e.g., *Zamora et al.*, 2009; *Blindow et al.*, 2012]. High-frequency radar sounders can measure ice thickness to within 10 m. To match that precision, airborne gravity is required to operate at the

submilligal (mGal) level: 1 mGal is 10^{-5} m^2/s. A gravity variation of 1 mGal corresponds to an unbound layer of bedrock increasing in thickness by 12.7 m, keeping the height of the ice surface constant [*Hinze et al.*, 2013]. The advent of advanced differential GPS processing techniques, combined with inertial navigation units, and more stable gravimeters developed for mineral and oil explorations has made it possible to achieve that level of precision from slow-moving, low-altitude, airborne platforms [*Argyle et al.*, 2000; *Studinger et al.*, 2008].

Here we employ the Sander Geophysics Ltd. AIRGrav gravity system to survey the NPI and SPI of South America. We describe the gravity data obtained over regular grids on the plateau and higher-resolution grids on select glaciers, and how we used these data to calculate ice thickness. We discuss how the results relate to the pattern of ice motion of the icefields, its regime of surface mass balance, and the implications for the glacier evolution and future contribution to sea level.

2. Data and Methods

In May and November 2012, we deployed the AIRGrav system in Patagonia, Chile, for periods of 4–6 weeks on Eurocopter AS-350 B2 and B3 helicopters. AIRGrav is an inertially referenced gravimeter that uses a Schuler-tuned inertial platform that supports three orthogonal accelerometers. Accelerometer data are recorded at 128 Hz and later decimated to 2 Hz in processing. AIRGrav delivers gravity data with a noise level better than 0.5 mGal with a half sine wave ground resolution of 2 km [*Studinger et al.*, 2008]. A Novatel OEM-V3, 14-channel GPS Satellites, 12-Channel Global Navigation Satellite System, 2-Channel Sbas, and 1-Channel L Band multifrequency receiver were used for GPS ground reference at Tortel (47.7854°S 073.5289°W, 22.5 m elevation) or Cochrane (47.2442°S 72.585°W, 224.7 m elevation). The GPS station on the aircraft used a Novatel DL-V3 integrated GPS receiver and data logger which provides averaged position and raw range information sampled every 0.1 s. The comparative navigation data supplied during all production flights allow for postprocessed differential GPS corrections for every survey flight. The helicopter carried a Riegl LD90-31K-HiP Laser Rangefinder, which is an eye-safe laser, with a range of 1500 m, an accuracy of 5 cm, and a data rate of 3.3 Hz. SGL proprietary geophysical software was used for AIRGrav data processing.

The traverse line spacing was 400 m, with a control line spacing of 2000 m (Figure 1). Target speed was 50 knots on the glaciers and 60 knots on the plateaus. All 21 flights were flown with a ground clearance of 80 m. NPI was divided between three high-resolution blocks over Glaciar San Rafael, San Quíntin, Steffen, and Colonia. The remainder of NPI was flown at lower resolution. NPI terrain varies from sea level to 4000 m. The southern area of the survey covered the northern half of SPI. The area was divided into three high-resolution blocks over Glaciar Jorge Montt, Occidental and Greve, and O'Higgins. The remainder of the area was flown at lower resolution. The terrain of this section of SPI varies between sea level and 3600 m. Adverse weather conditions prevented the survey of San Quíntin (NPI) and Greve (SPI). We surveyed a total area of 1950 km^2 (49%) of NPI and 3360 km^2 (30%) of SPI.

The gravity data were processed into free-air gravity anomaly after Eotvos, normal gravity, free-air, static, and level corrections. Statistical noise was reduced using a 20 s filter on the glacier data and 28 s on the plateau. Grids were generated at 200 m for the glaciers and the icefields (Figures 1c–1d). Two-dimensional cosine tapered low-pass filtering was applied to the grid to cancel out noise and achieve better noise reduction than would be possible by simply increasing the degree of line filtering. The glacier data acquired on a 500 m grid used a 750 m half-wavelength low-pass filter, whereas the plateau data acquired on a 2 km grid used a 1000 m filter. A repeat of the same line indicated a noise level of 0.8 to 1.4 mGal, which is the expected nominal precision of AIRGrav.

Rivera et al. [2012] collected seafloor bathymetry data in front of Jorge Montt in February 2010 from a zodiac using a Furuno sonar system, along with a Datasonic Bubble Pulser subbottom profiler. *Casassa et al.* [2007] used a parametrical echo sounder (Innomar) in 2004 and 2005 to sound Lake O'Higgins. *Koppes et al.* [2010] surveyed the bathymetry of Laguna San Rafael from a zodiac using a Datasonics Bubble Pulser combined with a Lowrance 18-C depth sounder. These bathymetry data were used to constrain the gravity modeling in fjords and lakes. We used a sediment thickness of 60 m at the center of Jorge Montt fjord following *Koppes et al.* [2015], decreasing to 0 m to the sides with a hyperbolic cosine law. We assumed a similar sediment thickness for Laguna San Rafael and Lago O'Higgins and verified a posteriori that this provided an excellent fit between observed and modeled gravity.

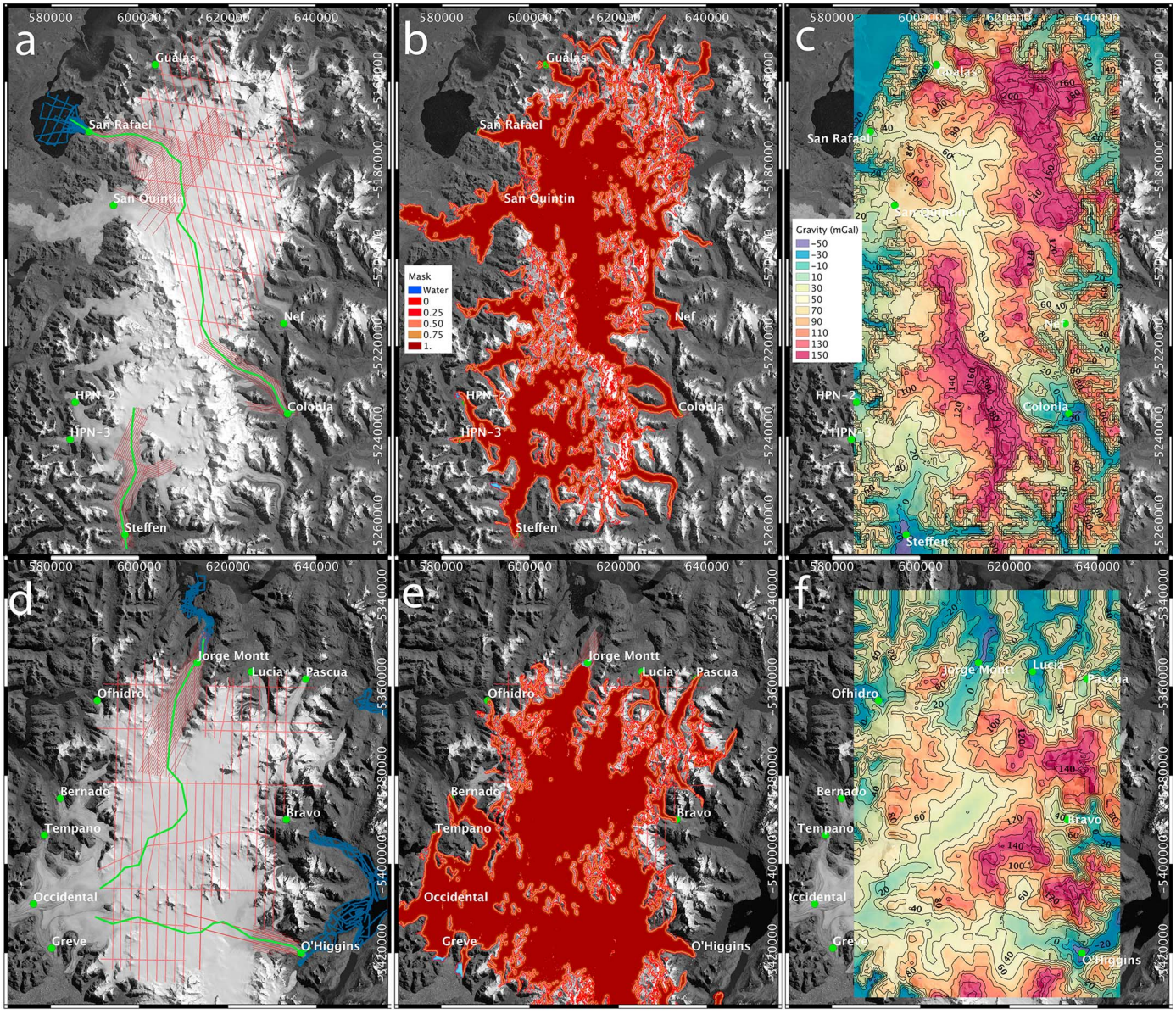

Figure 1. Airborne gravity survey lines and land-ice mask of the Northern (NPI) and Southern Patagonian Icefields (SPI). (a) Flight lines of AIRGrav (red), bathymetry data (blue) used for control in NPI ((d) SPI) and profiles used in Figure 3 (green). (b) Ice mask (values from 0 to 1) used to perform the gravity inversion in NPI ((e) SPI). 1 is fully inverted, 0 is not inverted. Landsat 7 image from year 2012 in the background. (c) Observed free-air gravity anomalies (mGal) within the survey domain completed with a forward model outside of the survey domain for NPI ((f) SPI).

We formed a three-dimensional model of NPI and SPI using the Geosoft GMSYS-3D software package which implements *Parker* [1973] method. The model included two layers on land: ice and bedrock with densities of 0.917 and 2.8 g/cm^3, respectively (same unit for all densities that follow). Beneath the ice, we used an initial estimate for the bedrock density, which was adjusted iteratively to obtain the best agreement between modeled and observed gravity, as discussed below. In the fjord, the model included three layers: seawater (1.03 density) or lake water (1.0 density), a layer of sediments with a density of 1.67, and bedrock (2.8 density). Surface reference is from laser altimetry acquired simultaneously with the gravity data. We also used Shuttle Radar Topography Mission (SRTM) data from year 2000 as background elevation for the entire icefields. All gravity data were upward continued to 3900 m on NPI and 3200 m on SPI, i.e., the highest elevation of the surveyed area. Results obtained with a different upward continuity elevation or different grid spacings were found to be identical (Figures 2a–2d).

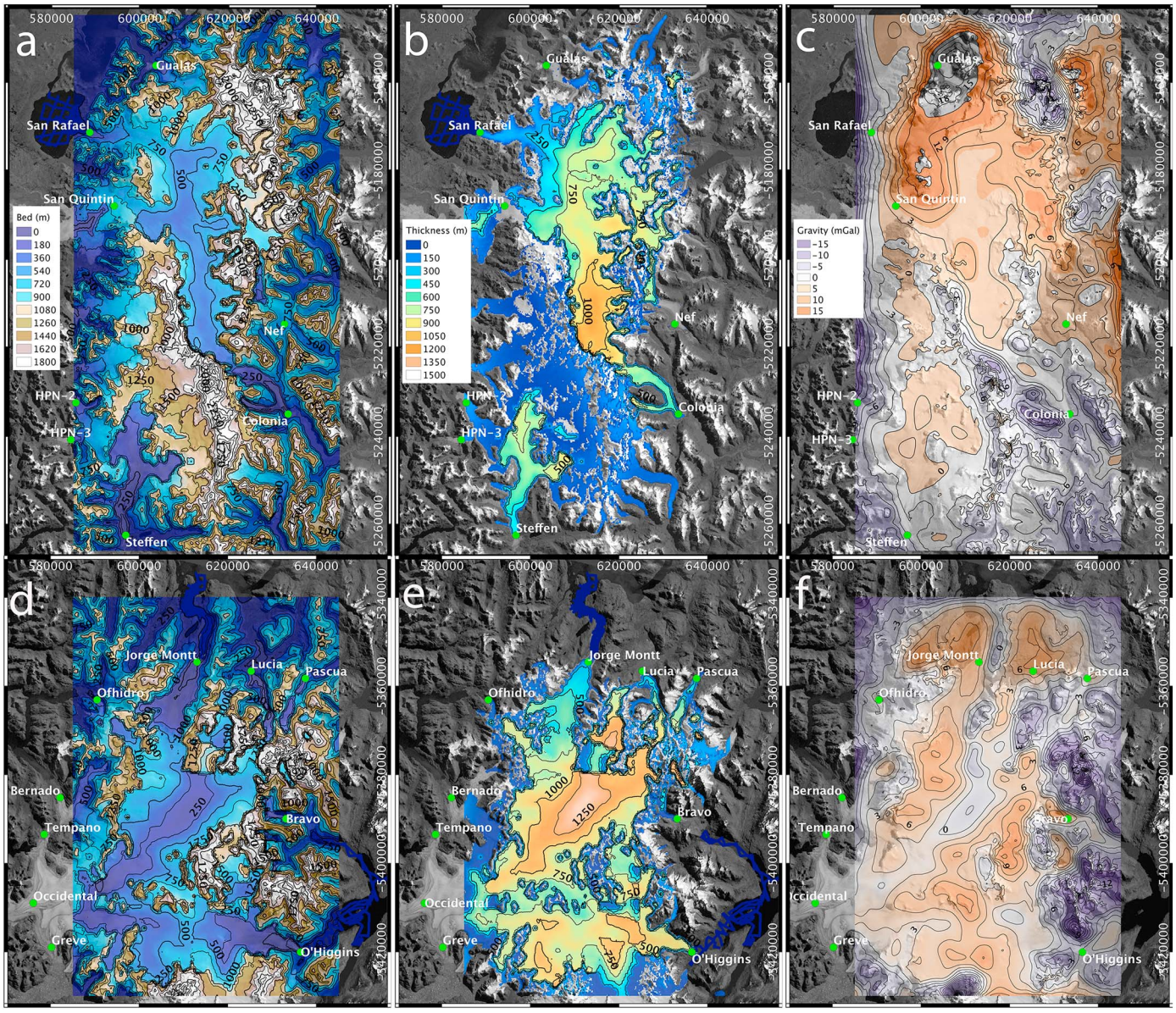

Figure 2. Bed elevation and ice thickness inferred from airborne gravity observations of the Northern (NPI) and Southern Patagonia Icefields (SPI). (a) Bed elevation (in meters above mean sea level) for NPI ((d) SPI); (b) ice thickness (meters of solid ice) for NPI ((e) SPI). (c) Gravity misfit between model and observation in milligal (mGal) for NPI ((f) SPI). A 1 mGal Bouguer anomaly corresponds to a 12.7 m height variation of the bed for an infinite plate of ice on rock with a constant surface elevation. Contour levels are every 250 m for bed elevation and thickness, and 3 mGal for gravity. A Landsat 7 image from year 2012 is in the background.

A trial and error procedure was employed to select the optimal density of bedrock. We measured the rate of conversion of the solution from the initial estimate with a density varying from 2.6 to 3.1. The results reveal a minimum at a density of 2.8 for both NPI and SPI (Figure S1 in the supporting information). This density minimum is consistent with the relative abundance of hornblende-biotite granite and metapelitic rock in the area [*Herve et al.*, 2007; *Motoki et al.*, 2006], with a density of 2.8. We adopted this bedrock density for the entire domain.

An ice mask was generated using a Landsat image from year 2012 (Figures 1e–1f). Over land ice, we derived an inversion coefficient varying between 0 and 1. With a value of zero, no data inversion is performed, i.e., we keep the initial solution. With a value of 1, ice thickness is inferred completely from the gravity data. With a value between 0 and 1, the solution is partially constrained by the gravity data. We employed surface slope from SRTM to constrain the values of the inversion coefficient. In areas of steep slopes, e.g., along mountain

flanks or near nunataks, the inversion coefficient is close to 0 because ice thickness should be small and the solution should not deviate significantly from the initial (small) value. Conversely, over the plateau, the inversion coefficient is chosen close to 1 (Figure 1b).

The quality of the initial solution for calculating ice thickness from gravity has an important effect on the rate of convergence to the final solution. To initialize the inversion, we applied a conversion factor of 10 m/mGal on the gravity anomalies, which is lower than the theoretical Bouguer anomaly of 12.7 m/mGal for an infinite layer of ice on bedrock because the icefields are of finite extent and exhibit significant spatial variations in ice thickness. Second, we also found that the gravity field outside of the surveyed area had an important impact on the solution as well, especially in the proximity of high mountain ranges. To account for that effect, we ran a forward model of the gravity field outside of the survey domain using the SRTM topography on land with a density of 2.8, a density of 1.0 on lakes, 1.03 in fjord waters, and an 800 m ice thickness in the southern part of SPI. A 1 km gap was used in between observations and forward model to insure a smooth transition of the modeled gravity toward the observed gravity. Using an external gravity field improved the quality of the solution in the glacier troughs. Inversion quality is quantified as the goodness of fit between the modeled gravity and the observed gravity (Figures 2e and 2f).

To translate the error in gravity into meters of ice, we used a conversion rate of 12.7 m/mGal on the plateaus and 20 m/mGal in the terminal valleys. These rates were determined from model fitting of two-dimensional profiles using Geosoft. We studied two cases: a flat plate of ice on bedrock and a smooth U-shaped valley filled with ice on top of bedrock. For a given height variation of the bedrock, we observed the corresponding change in computed gravity to obtain the conversion rate.

3. Results

The bed elevation and ice thickness of NPI and SPI are shown in Figure 2 with an intrinsic resolution 750 m for the glacier troughs and 1 km for the plateau. On the plateau, the modeled gravity fits observations within 3–5 mGal or 38–64 m of ice. The error increases in narrow valleys and away from survey lines to 9 mGal or 114 m of ice. At sea and on lakes, we obtain an excellent agreement between bed topography and bathymetry data, with a RMS difference of 20–30 m in Jorge Montt, including Lago O'Higgins and Laguna San Rafael where gravity and bathymetry data have minimal overlap (Figure 3). The inversion provides a seamless description of the bed elevation across the boundary between land ice and water.

Ice thickness exceeds 1 km in a large part of the NPI plateau, where the data reveal a deep trench running north-south from Glaciar San Rafael to Colonia (Figures 2 and 3). A comparison with ice velocity indicates that most ice flows along the trench toward the San Quíntin/San Rafael drainages to the west and toward the Colonia drainage to the east. The NPI plateau thickness values are in the same range as those calculated by *Casassa* [1987]. At the Equilibrium Line Altitude (ELA) of San Rafael (950–1000 m) [*Rivera et al.*, 2007], ice thickness is 400–500 m versus 650 m for San Quíntin (1000 m ELA), 900 m for Colonia (1300 m ELA), and 800 m for Steffen (980 m ELA). The relatively shallow thickness of San Rafael contrasts with that of the other glaciers and is a robust feature of the gravity inversion. San Rafael is estimated to be only 200–300 m thick near its terminus. This result is consistent with the cross-sectional area in *Koppes et al.* [2010]. In contrast, Colonia is 600 m thick about 4 km from its terminus and Steffen is 400 m thick near its front.

The basin of Glaciar Occidental, SPI, is underlaid by a trough about 1.5 km deep, oriented southwest-northeast, with the deepest ice in the upper reaches of Occidental and a bed elevation at sea level. In contrast, farther south, the bed elevation of the plateau separating Greve and O'Higgins rises 600 m above sea level. A comparison with ice velocity indicates that ice flow from Occidental is channelized along the trench (Figure S2). In the lower part of the glacier, Occidental branches out into Bernardo, Témpano, Occidental, and Greve (Figures S2–S3). At the edge of our survey, the bed of Occidental is near sea level with an ice thickness of 900 m. The bed of Greve is at 100 m elevation with 800 m of ice, but the survey does not extend to its proglacial lake. The drainage basins of this part of SPI were delineated with precision using ice flow data [*Mouginot and Rignot*, 2014]. Ice exceeds 600 m at 800 m elevation for Jorge Montt (ELA is about 880 m in *Casassa et al.* [2014]) on the northern side of SPI, 1000 m on Occidental on the west side (ELA = 1000 m), and 1000 m on O'Higgins (ELA = 1000 m) on the east. These depths exceed the reflecting horizon of ground radar sounding systems. Deeper ice is likely present farther, in "Paso Cuatro Glaciares" (smallest surface slope), at the divide between Glaciar Chico, O'Higgins, Pío XI, and Viedma [*Rivera and Casassa*, 2002].

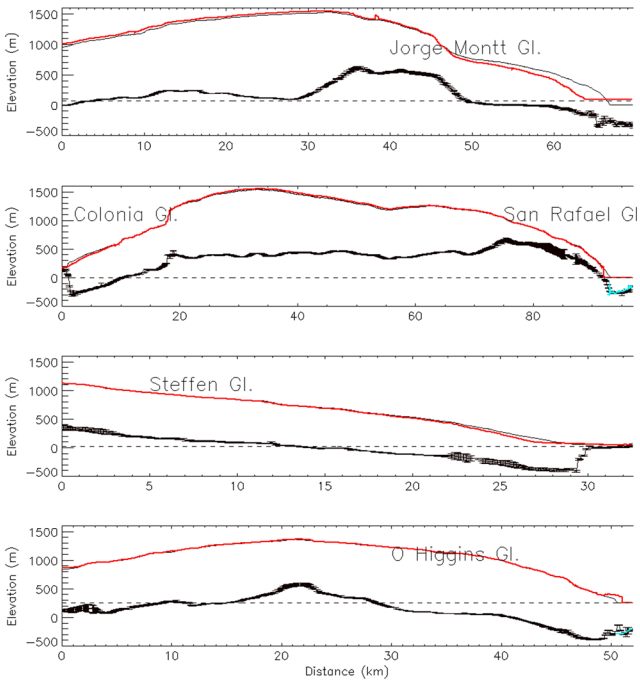

Figure 3. Comparison of the gravity-inferred bed elevation (red) with bathymetry control (blue) along profiles (green in Figure 1a) with year 2012 laser-derived surface elevation (light brown), and Shuttle Radar Topography Mission surface elevation data (in meters above mean sea level) from year 2000 (black). (first panel) Glaciar Jorge Montt, (second panel) Colonia/San Rafael, (third panel) Steffen, and (fourth panel) O'Higgins.

We calculate glacier ice fluxes in the proximity of the ELA of each glacier, where we have both gravity data and ice surface velocity (Figure S2 and Table 1). We vary the position of the fluxgate by ±400 m to calculate a mean flux after smoothing the velocity data to 720 m to match the resolution of the thickness data. We convert the flux into mass using a density of 0.917. The percentage error in flux is estimated from the sum of the percentage error in thickness and the percentage error in velocity. The largest error source is thickness. At each fluxgate, we assume that surface velocity is equivalent to a depth-averaged velocity. In Patagonia, deformation speeds are slow: a 700 m thick slab of temperate ice with 2% slope flows at 50 m/yr [*Mouginot and Rignot*, 2014]. Fast flow speeds (>500 m/yr) at the fluxgates are therefore entirely due to sliding. The results (Table 1)

Table 1. Ice Flux (in Gigatons per Year, 10^{12} kg/yr) at the Fluxgates in Figure S2 for Glaciar San Rafael, San Quíntin, Steffen-HPN2-HPN3 Combined, and Colonia for the Northern Patagonia Icefield (NPI), and Glaciar Jorge Montt, Occidental-Témpano-Greve Combined, and O'Higgins for the Southern Patagonia Icefield (SPI), Obtained by Combining Ice Thickness From This Study With Ice Velocity Data From *Mouginot and Rignot* [2014][a]

Glaciar	Elevation (m)	Ice flux (Gt/yr)	Area (km^2)	Balance (m/yr)
San Rafael	1190	1.37±0.2	523	2.6±0.3
San Quíntin	1130	1.75±0.2	422	4.1±0.5
Steffen, HPN2, and HPN3	1090	1.74±0.3	466	3.7±0.5
Colonia	1309	0.80±0.1	150	5.3±0.6
Jorge Montt	784	1.88±0.3	350	5.3±0.9
Occidental, Témpano, and Greve	950	3.27±0.4	842	3.9±0.5
O'Higgins	1140	2.57±0.3	727	3.5±0.4

[a]Elevation, mean elevation above mean sea level at the fluxgate in meters. Area, drainage area above the fluxgate in square kilometer. Balance, balance accumulation deduced by dividing the ice flux by the drainage area, in meters of water equivalent per year, with associated uncertainties.

indicate mass fluxes ranging from 0.8 ± 0.2 Gt/yr (Colonia), 1.4 ± 0.2 Gt/yr (San Rafael), 1.7 ± 0.3 Gt/yr (Steffen, HPN2, and HPN3), and 1.8 ± 0.2 Gt/yr (San Quíntin) for NPI, and 1.9 ± 0.3 Gt/yr (Jorge Montt), 2.6 ± 0.3 Gt/yr (O'Higgins), and 3.3 ± 0.4 Gt/yr (Greve, Occidental, and Témpano) for SPI. When compared with the drainage area above the fluxgates, we deduce annual balance accumulation levels of, respectively, 5.3 ± 1, 2.6 ± 0.3, 4.1 ± 0.5, and 3.7 ± 0.5 for NPI, and 5.3 ± 0.9, 3.9 ± 0.5, and 3.5 ± 0.4 m/yr water equivalent for SPI. These accumulation values are consistent with the limited ice core data collected in Patagonia [e.g., *Lenaerts et al.*, 2014] but are not directly comparable to point measurements. A comparison with output products from surface mass balance models is beyond the scope of this study.

4. Discussion

The inversion results suggest that the proglacial lakes in front of Glaciar Steffen and Colonia, in NPI, are more than 350 m deep. Lake bathymetry has never been measured in these proglacial environments. Nearby lakes, Lago Leones and Nef (NPI), however, have reported depths of 300 to 350 m [*Harrison et al.*, 2008; *Warren et al.*, 2001], so it is possible that Steffen and Colonia lakes are this deep. The recent retreat of these glaciers may have also deposited fresh sediments [*Koppes et al.*, 2015]. A deposition of a 60 m layer of fresh sediment would introduce a 100 m bias in inferred water depth.

Water depth in Lago O'Higgins is the greatest (800 m) recorded in South America [*Casassa et al.*, 1997, 2007]. The glacier underwent a spectacular 15 km retreat between 1896 and 1995 due to frontal detachment from a prominent island and subsequent retreat in an over deepened bed. The glacier is currently flowing at rapid speeds, >3 km/yr at the ice front [*Sakakibara and Sugiyama*, 2014], which is grounded in waters up to 480 m deep. The lake level is 252 m above mean sea level. The glacier bed remains below that lake level for another 20 km inland, which means that the glacier will continue to calve into lake waters for decades to come if it continues retreating at the current rate of 20–40 m/yr [*Sakakibara and Sugiyama*, 2014]. Similarly, Jorge Montt, which retreated 540 m/yr in 1988–2000 and 240 m/yr in more recent years, will remain below sea level for another 15 km from its current position before the bed rises above sea level. At the present rate of retreat, the glacier will continue to calve into ocean waters for another 60 years before detaching from the ocean.

On NPI, the bed of San Rafael is rising above sea level within 1 km of the 2012 ice front. If the glacier retreats further and loses contact with the relatively warm marine waters of the proglacial tidewater lagoon, we expect iceberg calving and subaqueous melting of the glacier by the ocean waters to cease, and the retreat of the glacier should be rapidly slow. This may already have been taking place since the glacier speed has dropped since 2006, and its retreat was negligible in 2007–2014 [*Mouginot and Rignot*, 2014] (Figure S1) compared to prior years.

On SPI, Greve ends in a shallow proglacial lake formed by the readvance of Glaciar Pío XI, while Occidental ends in a shallow proglacial lake near the ocean. Only Glaciar Témpano and Jorge Montt terminate in the ocean in this region. *Dowdeswell and Vasquez* [2013] report shallow waters in the front of Témpano, where the flow speed is low [*Mouginot and Rignot*, 2014] and Landsat imagery reveals many freshly deglaciated islands. About 15 km from its terminus, our data indicate that the glacier bed remains near sea level. Additional data are needed to determine if the glacier bed remains below sea level between the ice front and the edge of our survey.

The gravity survey must be complemented by additional data, e.g., radar sounding surveys, to provide higher-resolution, higher vertical precision data. The gravity-inferred ice thickness will constrain the interpretation of radar echoes, identify potential reflecting horizons, and help separate bed returns from off-nadir returns. Once well-evaluated surface mass balance reconstructions are available, the thickness data can be employed in combination with high-resolution ice motion vectors and ice thinning rates to reconstruct the entire icefield thickness using a mass conservation approach [*Morlighem et al.*, 2014].

Several reconstructions of surface mass balance (SMB) have been assembled recently for the Patagonia Icefields using high-resolution regional climate atmospheric models combined with downscaling or direct downscaling of reanalysis data [*Lenaerts et al.*, 2014; *Schaefer et al.*, 2015]. It is a challenge for these high-resolution reconstructions to reproduce the steep east-west mass balance gradients across the icefields associated with their rugged surface topography. Few field data are available to evaluate these models. Comparison of the balance accumulation levels that derived the combination of ice velocity and ice thickness

will eventually become instrumental in evaluating these surface mass balance models, but additional work is needed both in terms of ice thickness mapping and reliability of the SMB models to reach that level of comparison and model evaluation.

5. Conclusions

We present a first comprehensive mapping of ice thickness in the Patagonia Icefields in South America, which includes a significant fraction of NPI and the northern part of SPI. We find that ice thickness inferred from gravity data on the NPI and SPI plateaus exceeds the standard reflecting horizon of temperate ice radars (about 700 m), and hence, gravity data are an important complement to measure ice thickness. Ice in excess of 1 km is found throughout the NPI and SPI plateaus, or exceeding 1.5 km. Ice may be even thicker farther south. This study demonstrates the usefulness of modern airborne gravity techniques to probe temperate ice masses, especially on the plateaus, and provide fundamental, new information on bed elevation, ice thickness, and ice volume. This information is important to estimate the icefield volume, ice fluxes, mass balance, retreat potential, and reconstruct former extents of the icefields. Additional surveys are required to complete the coverage of SPI and fill in data gaps in NPI. More broadly, high-resolution airborne gravity surveys should benefit other parts of the world that are currently challenging to probe with radar sounders. This includes glaciers of coastal Alaska and also of southeast Greenland where high-frequency—and even low-frequency—radars are limited by the presence of a perennial layer of liquid water below the surface [*Forster et al.*, 2013] that prevents radar signals to reach the bed.

Acknowledgments
This work was performed at the University of California Irvine under grant 3280 from the Gordon and Betty Moore Foundation and at the Jet Propulsion Laboratory, California Institute of Technology under a grant with NASA. We thank R. Zamora and D. Ulloa from CECS for their assistance, and N. Glasser and one anonymous reviewer for comments on the manuscript. The gravity data are available upon request from the authors and at the National Snow and Ice Data Center, Boulder CO.

References

Argyle, M., S. Ferguson, L. Sander, and S. Sander (2000), AIRGrav results: A comparison of airborne gravity data with GSC test site data, *The Leading Edge*, *19*, 1134–1138.

Blindow, N., C. Salat, and G. Casassa (2012), Airborne GPR sounding of two deep temperate glaciers in the Northern Patagonia Icefield, in *Proceedings of the 14th International Conference on Ground Penetrating Radar (GPR 2012)*, Tongji Univ., Shanghai, China.

Casassa, G. (1987), Ice thickness deduced from gravity anomalies on Soler Glacier, Nef Glacier and the Northern Patagonia Icefield, *Bull. Glacier Res.*, *4*, 43–57.

Casassa, G., H. Brecher, A. Rivera, and M. Aniya (1997), A century-long recession record of Glacier O'Higgins, Chilean Patagonia, *Ann. Glaciol.*, *24*, 106–110.

Casassa, G., et al. (2007), *Lago O'Higgins, Patagonia: Glacial Over Deepening and Glacier Retreat in a Freshwater Fjord*, Geosur, Valdivia, Chile.

Casassa, G., J. L. Rodriguez, and T. Loriaux (2014), A new glacier inventory for the Southern Patagonia Icefield and areal changes 1986–2000, Chap 27, in *Global Land Ice Measurements From Space*, edited by J. S. Kargel et al. Springer Praxis Books, Springer, Berlin, Germany.

Dowdeswell, J. A., and M. Vasquez (2013), Submarine landforms in the fjords of southern Chile: Implications for glacimarine processes and sedimentation in a mild glacier-influenced environment, *Quat. Sci. Rev.*, *64*, 1–19.

Forster, R., et al. (2013), Extensive liquid meltwater storage in firn within the Greenland ice sheet, *Nat. Geosci*, *7*, 95–98.

Glasser, N. F., S. Harrison, K. N. Jansson, K. Anderson, and A. Cowley (2011), Global sea-level contribution from the Patagonian Icefields since the Little Ice Age maximum, *Nat. Geosci.*, *4*, 303–307.

Harrison, S., N. Glasser, V. Winchester, E. Haresign, C. Warren, G. A. T. Duller, R. Bailey, S. Ivy-Ochs, K. Jansson, and P. Kubik (2008), Glaciar Leon, Chilean Patagonia: Late-Holocene chronology and geomorphology, *The Holocene*, *18*(4), 643–652.

Herve, F., R. J. Pankhurst, C. M. Fanning, M. Calderon, and G. M. Yaxley (2007), The South Patagonian batholith: 150 my of granite magmatism on a plate margin, *Lithos*, *97*, 373–394.

Hinze, W. J., R. R. B. von Freze, and A. H. Saad (2013), *Gravity and Magnetic Exploration: Principles, Practices and Applications*, Cambridge Univ. Press, Cambridge, U. K.

Koppes, M., R. Sylwester, A. Rivera, and B. Hallet (2010), Sediment yields over an advance-retreat cycle of a calving glacier, Laguna San Rafael, North Patagonian Icefield, *Quat. Res.*, *73*, 84–95.

Koppes, M., B. Hallet, E. Rignot, J. Mouginot, J. Smith Wellner, and K. Bolt (2015), Observed latitudinal variations in erosion as a function of glacier dynamics, *Nature*, *526*, 100–103.

Lenaerts, J. T. M., M. van den Broeke, J. M. van Wessem, and W. J. van de Berg (2014), Extreme precipitation and climate gradients in Patagonia revealed by high-resolution regional atmospheric climate modeling, *J. Clim.*, *27*, 4607–4621.

Motoki, A., Y. Orihashi, J. A. Naranjo, D. Hirata, P. Skvarca, and R. Anma (2006), Geologic reconnaissance of Lautaro Volcano, Chilean Patagonia, *Revista Geologica de Chile*, *33*(1), 177–187.

Mouginot, J., and E. Rignot (2014), Ice motion of the Patagonia Icefields of South America: 1984–2014, *Geophys. Res. Lett.*, *42*(5), 1441–1449, doi:10.1002/2014GL062661.

Mouginot, J., E. Rignot, Y. Gim, and D. Kirchner (2014), Low-frequency radar sounding in Antarctica and Southern Greenland, *Ann. Glaciol.*, *55*(67), 138–146.

Morlighem, M., E. Rignot, J. Mouginot, H. Seroussi, and E. Larour (2014), Deeply incised submarine glacial valleys beneath the Greenland Ice Sheet, *Nat. Geosci.*, *7*, 418–422.

Parker, R. L. (1973), The rapid calculation of potential anomalies, *Geophys. J. Int.*, *31*, 447–455.

Raymond, C. F., T. A. Neumann, E. Rignot, K. Echelmeyer, A. Rivera, and G. Casassa (2005), Retreat of Glaciar Tyndall, Patagonia, over the last half-century, *J. Glaciol.*, *51*(173), 239–247.

Rignot, E., A. Rivera, and G. Casassa (2003), Contribution of the Patagonia Icefields of South America to sea level rise, *Science*, *302*, 434–437.

Rivera, A., and G. Casassa (2002), Ice thickness measurements on the Southern Patagonia Icefield, in *The Patagonian Icefields: A Unique Laboratory for Environmental and Climate Change Studies, Series of the Centro de Estudios Cientificos*, edited by G. Casassa, F. Sepulveda, and R. Sinclair, pp. 101–115, Springer, New York.

Rivera, A., T. Benham, G. Casassa, J. Bamber, and J. A. Dowdeswell (2007), Ice elevation and areal changes of glaciers from the Northern Patagonia Icefield, Chile, *Global Planet. Change*, *59*, 126–137.

Rivera, A., J. Corripio, C. Bravo, and S. Cisternas (2012), Glaciar Jorge Montt (Chilean Patagonia) dynamics derived from photos obtained by fixed cameras and satellite image feature tracking, *Ann. Glacio.*, *53*(60), 147–155.

Rott, H., M. Stuefer, A. Siegel, P. Skvarca, and A. Eckstaller (1998), Mass fluxes and dynamics of Moreno Glacier, Southern Patagonia Icefield, *Geophys. Res. Lett.*, *25*(9), 1407–1410.

Sakakibara, D., and S. Sugiyama (2014), Ice-front variations and speed changes of calving glaciers in the Southern Patagonia Icefield from 1984 to 2011, *J. Geophys. Res. Earth Surface*, *119*, 2541–2554, doi:10.1002/2014JF003148.

Schaefer, M., H. Machguth, M. Falvey, G. Casassa, and E. Rignot (2015), Quantifying mass balance processes on the Southern Patagonia Icefield, *The Cryosphere*, *9*, 25–35.

Studinger, M., R. Bell, and N. Frearson (2008), Comparison of AIRGrav and GT-1A airborne gravimeters for research applications, *Geophysics*, *73*(6), 151–161.

Willis, M. J., A. K. Melkonian, M. E. Pritchard, and A. Rivera (2012a), Ice loss from the Southern Patagonian Ice Field, South America, between 2000 and 2012, *Geophys. Res. Lett.*, *39*(17), L17501, doi:10.1029/2012GL053136.

Willis, M. J., A. K. Melkonian, M. E. Pritchard, and J. M. Ramage (2012b), Ice loss rates at the Northern Patagonian Ice Field derived using a decade of satellite remote sensing, *Remote Sens. Environ.*, *117*, 184–198.

Warren, C., D. Benn, V. Winchester, and S. Harrison (2001), Buoyancy-driven lacustrine calving, Glaciar Nef, Chilean Patagonia, *J. Glaciol.*, *47*(156), 135–146.

Zamora, R., D. Ulloa, G. Garcia, R. Mella, J. Uribe, J. Wendt, A. Rivera, G. Gacitua, and G. Casassa (2009), Airborne radar sounder for temperate ice: Initial results from Patagonia, *J. Glaciol.*, *55*(191), 507–512.